nature materials

Article

https://doi.org/10.1038/s41563-023-01646-6

In situ PEGylation of CART cells alleviates cytokine release syndrome and neurotoxicity

Received: 8 May 2022

Accepted: 18 July 2023

Published online: 11 September 2023

Check for updates

Ningqiang Gong ¹⁷, Xuexiang Han ¹⁷, Lulu Xue ¹⁷, Rakan El-Mayta ¹, Ann E. Metzloff 1, Margaret M. Billingsley, Alex G. Hamilton 1, Michael J. Mitchell

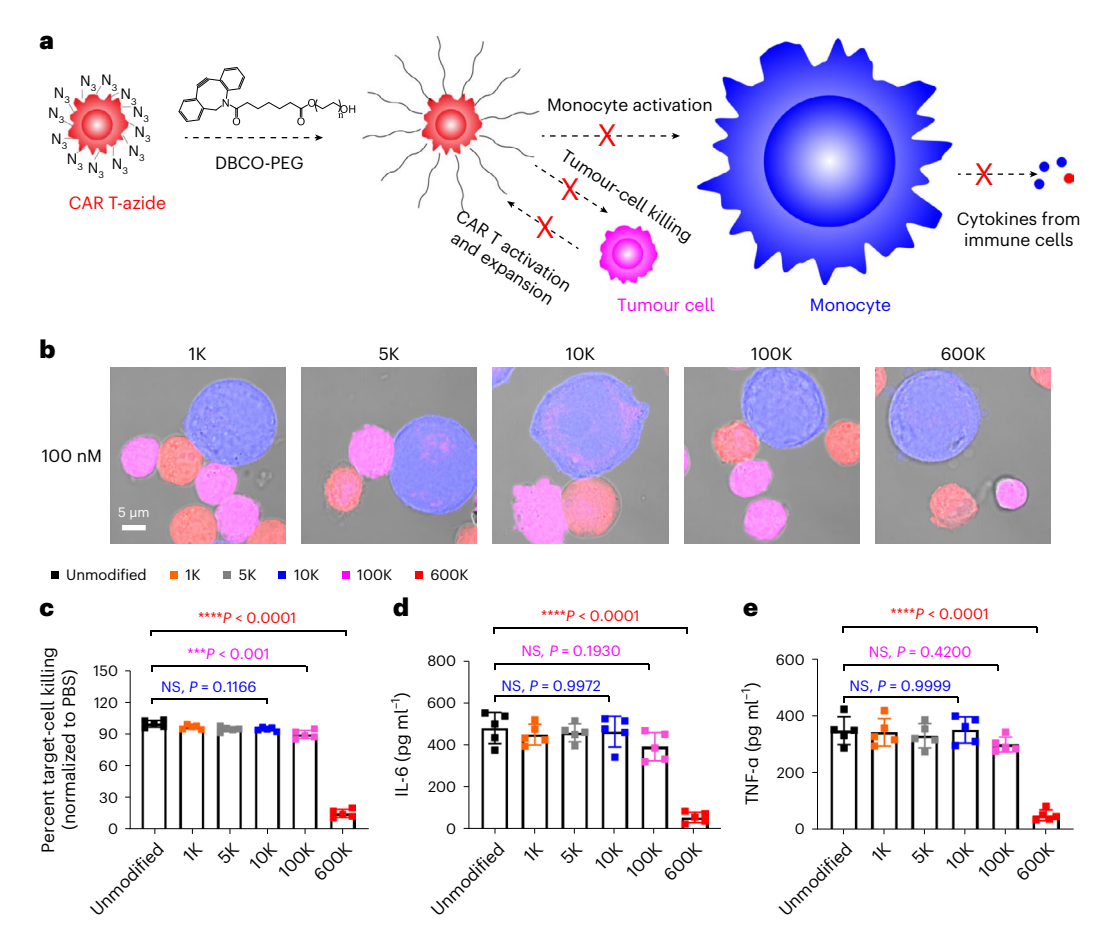
1,2,3,4,5,6

Chimeric antigen receptor T (CART) cell immunotherapy is successful at treating many cancers. However, it often induces life-threatening cytokine release syndrome (CRS) and neurotoxicity. Here, we show that in situ conjugation of polyethylene glycol (PEG) to the surface of CAR T cells ('PEGylation') creates a polymeric spacer that blocks cell-to-cell interactions between CART cells, tumour cells and monocytes. Such blockage hinders intensive tumour lysing and monocyte activation by CAR T cells and, consequently, decreases the secretion of toxic cytokines and alleviates CRS-related symptoms. Over time, the slow expansion of CAR T cells decreases PEG surface density and restores CART cell-tumour-cell interactions to induce potent tumour killing. This occurs before the restoration of CART cell-monocyte interactions, opening a therapeutic window for tumour killing by CART cells before monocyte overactivation. Lethal neurotoxicity is also lower when compared with treatment with the therapeutic antibody to cilizumab, demonstrating that in situ PEGylation of CART cells provides a materials-based strategy for safer cellular immunotherapy.

Chimeric antigen receptor T (CART) cell immunotherapy is a revolutionary cancer treatment technique^{1,2}. There are six CART cell therapies that have been approved by the US Food and Drug Administration (FDA) and a variety of candidates currently being assessed in clinical or preclinical studies^{3,4}. CAR T cells targeting CD19 have shown remarkable anti-tumour efficacy against B cell malignancies⁵⁻⁷. However, treatment often induces cytokine release syndrome (CRS)^{8,9} and neurotoxicity^{10,11}. Studies have shown that 20-70% of patients receiving CD19 CART cell therapy develop CRS^{12,13}. Severe CRS usually develops within a day after CART cell injection, with symptoms such as high fever, vomiting, and cardiovascular and respiratory insufficiency¹⁴⁻¹⁶. If left untreated, this can result in multiple organ dysfunction or patient death 17,18. CRS is also accompanied by neurotoxicity¹³. However, neurotoxicity is usually delayed for weeks after the disappearance of CRS-related symptoms and may induce patient death 19,20. To cilizumab, an anti-IL-6 receptor (IL-6R) antibody, is effective at CRS management in the clinical setting^{21,22} but has failed at preventing neurotoxicity^{19,23}.

Recently, several studies have demonstrated that monocytes/macrophages play a vital role in the development of these adverse conditions^{24–26} (Supplementary Fig. 1) with increased numbers of monocytes

Department of Bioengineering, University of Pennsylvania, Philadelphia, PA, USA. Penn Institute for RNA Innovation, Perelman School of Medicine, University of Pennsylvania, Philadelphia, PA, USA. 3 Abramson Cancer Center, Perelman School of Medicine, University of Pennsylvania, Philadelphia, PA, USA. ⁴Institute for Immunology, Perelman School of Medicine, University of Pennsylvania, Philadelphia, PA, USA. ⁵Cardiovascular Institute, Perelman School of Medicine, University of Pennsylvania, Philadelphia, PA, USA. 6 Institute for Regenerative Medicine, Perelman School of Medicine, University of Pennsylvania, Philadelphia, PA, USA. 7These authors contributed equally: Ningqiang Gong, Xuexiang Han, Lulu Xue. 🖂 e-mail: mjmitch@seas.upenn.edu



 $\label{lem:fig.1} \textbf{Fig. 1} | \textbf{PEGylation of CAR T cells alters cell-to-cell interactions and cytokine release. a-e, Schematic showing how conjugation of DBCO-PEG to azido-glycan modified CAR T cells affects cell-to-cell interactions. a, PEGylated CAR T cells (red) were co-incubated with both Raji tumour cells (pink) and monocytes (blue) for 4 h and cells were examined under confocal microscopy (b). c, Raji target-cell$

viability. **d**, Monocyte cytokine IL-6 concentration and **e**, T cell cytokine TNF- α concentration in cell-culture media were measured. Data in **c**, **d** and **e** are shown as mean \pm s.d. (n = 5 biologically independent experiments, one-way ANOVA with Tukey's post hoc test). P values are indicated (blue: 10K versus unmodified; pink: 100K versus unmodified; red: 600K versus unmodified).

in humanized mice associated with severe CRS²⁵. Moreover, overactivation of monocytes/macrophages is a source of toxic cytokines such as IL-6 and IL-1 that induce CRS and neurotoxicity^{25,27}. While CAR T cells failed to cause CRS in monocyte-depleted mice, anti-tumour efficacy was also attenuated²⁵, indicating monocytes may be necessary for effective CART cell therapy. Collectively, these findings highlight the complex role of monocytes in CART cell therapy as they are simultaneously crucial for CART cell-mediated toxicity and tumour-cell killing. Studies have shown that the overactivation of monocytes during CRS is a result of unwanted CART cell-monocyte interactions²⁸. For example, T cell surface proteins CD40 ligand 24,29,30, CD69 (ref. 31), lymphocyte activation gene³², and membrane-expressed TNF- α (refs. 33,34) can activate monocytes and macrophages via cell-to-cell interaction mechanisms^{28,35,36}. Therefore, decreasing monocyte overactivation via control of CART cell-monocyte interactions could provide a potential solution for the treatment of CRS and neurotoxicity.

Here, we validated in situ PEGylation on the surface of CAR T cells as a potential way to abolish the overactivation of monocytes by CAR T cells during CRS and prevent subsequent inflammatory effects by blocking cell-to-cell interactions between CAR T cells, monocytes and tumour cells.

PEGylation blocks cell-to-cell interactions in vitro

We first evaluated whether modification of CAR T cells with polyethylene glycol (PEG) can block cell-to-cell interactions in vitro. PEG was chosen as the polymeric spacer because it is a biomaterial that has

been FDA-approved for various biomedical applications³⁷. Human CD19-targeted CAR T cells were prepared, and CAR expression was evaluated (Supplementary Fig. 2)³⁸. Metabolic labelling was utilized to label the surface of CART cells with azide groups³⁹ by culturing CAR T cells with azido glycans (*N*-azidoacetylmannosamine-tetraacylated. Ac4ManNAz) for 48 h (Supplementary Fig. 3). The metabolic labelling strategy was found to be non-toxic⁴⁰ and did not affect the tumour-cell killing capacity of CART cells (Supplementary Fig. 4). To conjugate PEG to azide-labelled CART cells, dibenzocyclooctyne (DBCO)-modified PEG was synthesized⁴¹ (Supplementary Fig. 5). The DBCO group reacts with the azide group present on the CART cell surface under culture conditions⁴² (Fig. 1a) or in living animals⁴³. DBCO-PEGs with molecular weights (MWs) of 1,000 (1K), 5,000 (5K), 10,000 (10K), 100,000 (100K) and 600,000 (600K) were used to modify CART cells (Supplementary Fig. 6). We found that PEGylated CART cells with PEGs of MW1K, 5K, 10K and 100K were able to bind to anti-CD3 antibody-coated 96-well plates, but PEGylated CART cells with a PEG of MW 600K failed to bind to the well plate (Supplementary Fig. 6a,b), demonstrating that PEG600K can potentially be used to block cell-to-cell interactions (Supplementary Fig. 6a,b). Confocal images (Fig. 1b) showed that PEGylated CAR T cells with PEGs of MW 1K, 5K, 10K and 100K failed to block interactions between CART cells, Raji tumour cells and monocytes, whereas PEGylated CAR T cells with a PEG MW of 600K substantially blocked all cell-to-cell interactions (Fig. 1b). Moreover, PEG600K modification also decreased target tumour-cell killing (Fig. 1c). The levels of IL-6, a cytokine produced by activated monocytes/macrophages, and TNF- α ,

a cytokine produced by activated CAR T cells, were also substantially decreased (Fig. 1d,e). Further, we found that PEG600K modification did not induce CAR T cell toxicity (Supplementary Fig. 6c–e). These results suggest that modification of CAR T cells with PEG600K block cell-to-cell interactions and decrease both monocyte activation and cytokine release in vitro. Encouraged by these data, we sought to test whether PEGylation of CAR T cells in vivo may reduce CRS.

Conjugation of PEG to the surface of CAR T cells in vivo

We first constructed a humanized mouse model following a previous report (Supplementary Fig. 7a-i)²⁵. We then constructed a CRS model in tumour-bearing mice and demonstrated that CAR T cell infusion induced severe CRS in vivo (Supplementary Fig. 8a-m). Before testing whether DBCO-PEG600K can conjugate to CAR T-azide cells in mice, we first evaluated the expansion levels of CART cells in vivo. Because azide-labelled CAR T cells may divide after infusion¹⁹, it may affect DBCO-PEG600K conjugation. We found that in the low, medium and high tumour burden groups, CART cells had expanded by approximately one-and-a-half, two and six times at day 7 (peak expansion), respectively (Supplementary Fig. 9a-c). We further demonstrated that after one, six or even 20 times expansion, PEGylation was unaffected and prevented binding of CART cells to an antibody-coated plate (Supplementary Fig. 9d). These data illustrate that the azide group modification on the surface of CART cells is sufficient for DBCO-PEG600K conjugation even after CART cell expansion.

We then sought to investigate whether DBCO-PEG600K can conjugate to CAR T-azide cells in vivo. We first tested the biocompatibility of DBCO-PEG600K using a haemolysis assay (Supplementary Fig. 10). We then investigated the blood circulation of a Cy7-labelled DBCO-PEG600K (DBCO-PEG600K-Cy7) and found that DBCO-PEG600K-Cy7 has a 18 h half-life in the bloodstream in normal mice (Fig. 2a,b), and it spreads throughout the whole body after injection (Fig. 2c), which is similar to previous reports⁴⁴. We also investigated whether DBCO-PEG600K-Cy7 can conjugate to fluorophore (CSFE)-modified CAR T-azide cells in vivo (Fig. 2d-i). CAR T-CSFE cells were mainly detected in the liver, spleen and lymph nodes (Fig. 2d,e), which are the tissues where tumour cells localize. Cy7 signal was also detected in these tissues, indicating potential conjugation of DBCO-PEG600K-Cy7 to CAR T-azide cells (Fig. 2d,e). A flow cytometry experiment (Fig. 2f-m) showed that DBCO-PEG600K-Cv7 conjugated to CAR T cells in the blood circulation, liver, spleen and lymph node within 60 min (Fig. 2f-m). These results demonstrate the rapid conjugation of DBCO-PEG600K to CAR T-azide cells in vivo.

PEGylation of CART cells alleviates cytokine release syndrome

Next, we constructed a Raji tumour-bearing mouse model and intravenously (i.v.) infused CAR T-azide cells at day 0 (Supplementary Fig. 11a). After 24 h, all mice developed high fever ($\Delta T > 2$ °C, T: temperature). Immediately following high fever, DBCO-PEG600K at different doses (0, 1, 5, 10, 50 mg kg⁻¹) was i.v. injected into mice. We found that a low dose of DBCO-PEG600K (1 and 5 mg kg⁻¹) did not affect weight loss, body temperature and cytokine release compared with a phosphate-buffered saline (PBS) infusion (Supplementary Fig. 11b-g). Excitingly, higher doses of DBCO-PEG600K (10 and 50 mg kg⁻¹) greatly reversed weight loss, high fever and cytokine release (Supplementary Fig. 11b-g). To investigate the mechanism, we sorted CART cells from mouse blood at day 7 and cocultured them with luciferase and green fluorescence protein (GFP)-expressing Raji (Raji-Luc-GFP) cells and human monocytes for 24 h. CART cells sorted from mice that received 0,1 and 5 mg kg⁻¹ DBCO-PEG600K induced substantial Raji-Luc-GFP cell lysis and the production of both IL-6 and TNF-α (Supplementary Fig. 11h-j). However, CART cells collected from mice receiving 10 and 50 mg kg⁻¹DBCO-PEG600K exhibited very

low levels of target-cell killing and decreased cytokine production (Supplementary Fig. 11h–j). These results suggest the potential of a 10 and 50 mg kg $^{-1}$ injection of DBCO-PEG600K for controlling CRS in vivo. Since injections of 10 mg kg $^{-1}$ and 50 mg kg $^{-1}$ of DBCO-PEG600K displayed similar effects in decreasing CRS symptoms, we dosed mice with 10 mg kg $^{-1}$ of DBCO-PEG600K for all remaining studies.

Next, we investigated whether PEG600K must be conjugated to CART cells and whether a short DBCO-PEG could have a similar effect. We generated the CRS mouse model (Fig. 3a), and upon observation of high fever (Fig. 3b), 10 mg kg⁻¹DBCO-PEG1K, unmodified PEG600K and DBCO-PEG600K were injected i.v. into mice. As expected, treatment with DBCO-PEG1K and unmodified PEG600K did not affect weight loss, temperature or cytokine release compared with a PBS infusion (Fig. 3c-i). However, DBCO-PEG600K treatment greatly reversed weight loss, high fever and cytokine release (Fig. 3c-i). The number of CART cells, tumour cells and monocytes in mouse blood was also measured (Fig. 3j-l). In both DBCO-PEG1K- and unmodified PEG600K-treated mice, almost all tumour cells were cleared within 2-3 days post-CART cell administration. However, in animals treated with DBCO-PEG600K there was a significant delay in tumour-cell clearance, but all tumour cells were eventually cleared at day 35 post-CAR T cell injection (Fig. 3j,p,q). Along with the clearance of tumour cells, we found a rapid increase in CART cell and CD14⁺ monocyte numbers in the PBS, DBCO-PEG1K, and PEG600K groups (Fig. 3k,l). However, in mice treated with DBCO-PEG600K, CAR T cell and CD14⁺ monocyte expansion was greatly reduced (Fig. 3k,l). Moreover, the amount of IL-6⁺, IL-1⁺ and TNF-α⁺ monocytes at day 7 was greatly decreased in mice treated with DBCO-PEG600K compared with those in the PBS-, PEG600K- or DBCO-PEG1K-treated mice (Supplementary Fig. 12a-j). Since monocyte activation is a well-known sign of CRS, these results provide further support for the use of this PEGylation strategy in alleviating CRS-related symptoms.

To further verify whether the polymeric spacer is present on azide-labelled CAR T cell surfaces after DBCO-PEG600K injection, we sorted CAR T cells from treated mice and performed the three-cell coculture experiment mentioned previously. We found that CAR T cells isolated from mice that received DBCO-PEG1K and unmodified PEG600K induced substantial Raji-Luc-GFP cell lysis and cytokine release, whereas CAR T cells collected from DBCO-PEG600K-treated mice did not lead to high target-cell killing and cytokine release (Fig. 3m,n,o). Confocal images of CAR T cells from mice treated with DBCO-PEG600K that were cocultured with tumour cells and monocytes suggested that cell-to-cell interactions were blocked (Supplementary Fig. 13a). These results support DBCO-PEG600K-induced CRS alleviation due to the conjugation of DBCO-PEG600K to CAR T cells.

We further explored why tumour cells were eventually cleared even after the PEG spacer blocked cell-to-cell interactions. We found that CAR T cell expansion in vivo induced dilution of the PEG spacer (Supplementary Fig. 13b-g). We also cocultured these sorted cells with both Raji-Luc-GFP cells and monocytes and found that in the DBCO-PEG600K-treated group, CART cells collected at day 10 did not induce tumour-cell killing and cytokine (IL-6, IL-1, TNF-α) release compared with other groups (Supplementary Fig. 14a-h), indicating that cell-to-cell interactions were still blocked at day 10. However, the CAR T cells collected on days 15 and 20 induced substantial target-cell killing and cytokine release (Supplementary Fig. 14a-h). We believe that, as $DBCO\text{-}PEG600K \, became \, gradually \, diluted \, on \, the \, surface \, of \, CART \, cells, \, and \, constant \, cells \, and \, cells \, are the constant \, cells \, and \, cells \, are the constant \, cells \, are the co$ cell-to-cell interactions were gradually restored. Interestingly, at day 15, CART cells induced substantial tumour-cell killing and release of CAR T cell-associated cytokine TNF- α , but not monocyte-related cytokines (IL-6 and IL-1), suggesting the restoration of CAR T cell-tumour-cell interactions (day 15) before the recovery of CAR T cell-monocyte interactions (day 20). This is likely due to the smaller size of the Raji tumour cells (7–10 μm) and T cells (5–8 μm) compared with monocytes (30-50 µm). The size-dependent sequential cell-to-cell interaction

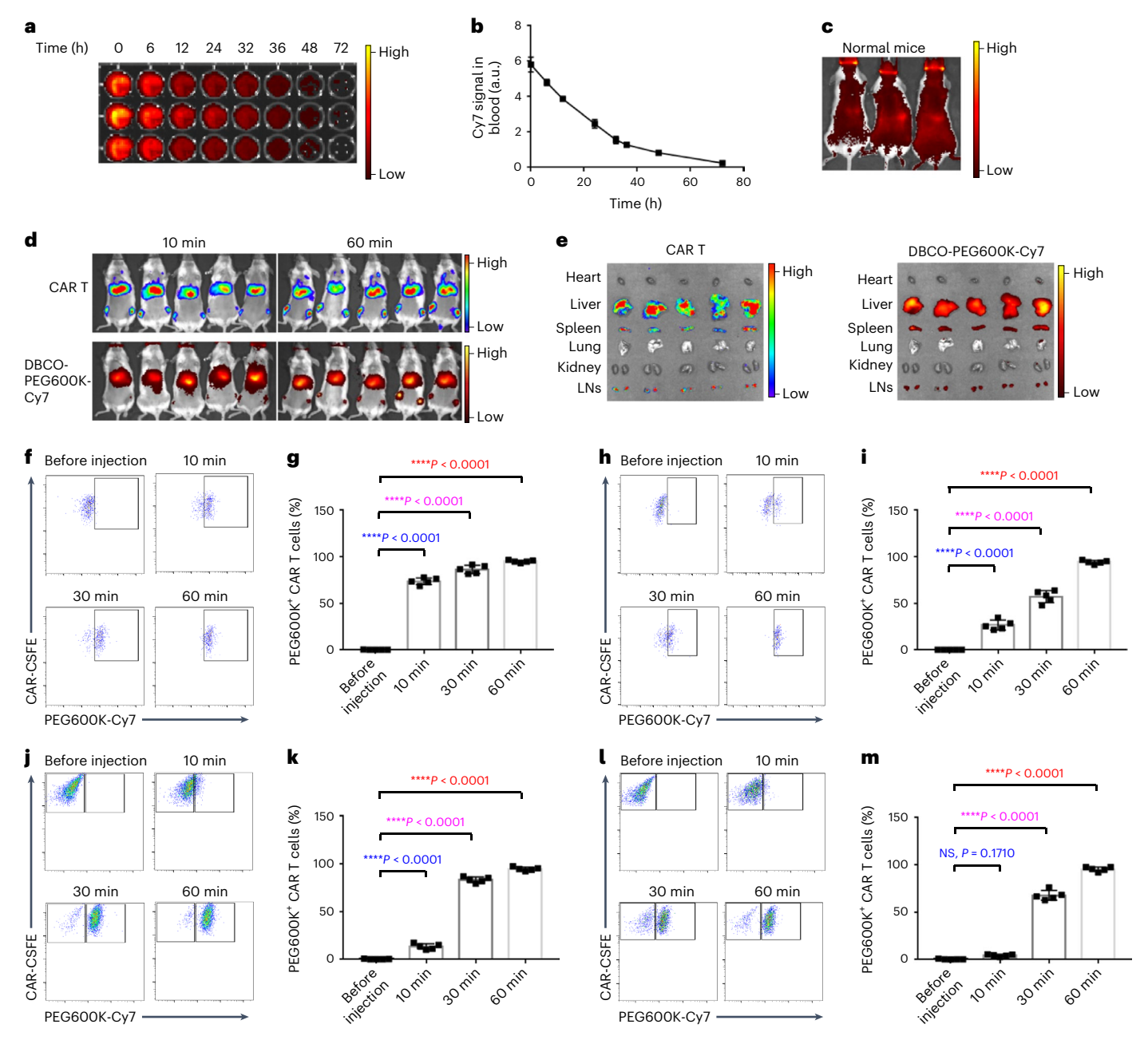


Fig. 2| **Conjugation of DBCO-PEG600K to CAR T cells in vivo. a**, Cy7-labelled DBCO-PEG600K (DBCO-PEG600K-Cy7) was i.v. injected into normal mice and 10 μL of peripheral blood was collected at various time points (0 h, 6 h, 12 h, 24 h, 32 h, 36 h, 48 h and 72 h) and the Cy7 signal in the blood was detected using IVIS. **b**, quantification of **a**. Data in **b** are shown as mean \pm s.d. (n = 3 biologically independent animals). **c**, Whole-body IVIS images of mice were taken 6 h following injection. **d**, Fluorophore (CSFE)-labelled CAR T cells (CAR T-CSFE) were used to treat tumour-bearing mice and the biodistribution of CAR T cells and DBCO-PEG600K-Cy7 in vivo were examined. **e**, Mouse hearts, livers, spleens, lungs, kidneys and lymph nodes were isolated and imaged using

IVIS. Mouse blood, lymph nodes (LNs), liver and spleen were collected before injection, 10 min, 30 min and 60 min after injection. \mathbf{f} - \mathbf{m} , The conjugation of DBCO-PEG600K-Cy7 to CAR T cells in the blood (\mathbf{f} , \mathbf{g}), liver (\mathbf{h} , \mathbf{i}), spleen (\mathbf{j} , \mathbf{k}) and LNs (\mathbf{l} , \mathbf{m}) was investigated using flow cytometry. Representative dot plots show the conjugation of DBCO-PEG600K-Cy7 to CAR T cells in the blood (\mathbf{f}), liver (\mathbf{h}), spleen (\mathbf{j}) and LNs (\mathbf{l}) at indicated time points. Quantification of Cy7⁺ CAR T cells in the blood (\mathbf{g}), liver (\mathbf{i}), spleen (\mathbf{k}), and LNs (\mathbf{m}). The data in \mathbf{g} , \mathbf{i} , \mathbf{k} , \mathbf{m} are shown as mean \pm s.d. (n = 5 biologically independent animals, one-way ANOVA with Tukey's post hoc test). P values are indicated (blue: 10 min versus before injection; pink: 30 min versus before injection; red: 60 min versus before injection).

restoration was also confirmed with an in vitro DBCO-PEG600K density experiment (Supplementary Fig. 15).

CAR T cell expansion in vivo is highly dependent upon the recognition of tumour cells. However, in our study, the DBCO-PEG600K modification blocked CAR T cell–tumour-cell interactions, and thus tumour cells could not induce rapid PEGylated CAR T cell expansion. Nevertheless, we found that DBCO-PEG600K-modified CAR T cells slowly expand in response to tumour-cell lysate (Supplementary Fig. 16),

allowing for the slow dilution of PEG on the CAR T cell surface to enable tumour-cell killing before the initiation of CAR T cell-induced monocyte activation.

PEGylation of CART cells alleviates neurotoxicity

Even though tocilizumab is effective at alleviating some symptoms related to severe CRS⁴⁵, it has failed to treat neurotoxicity⁴⁶. We sought to investigate whether a DBCO-PEG600K injection has advantages

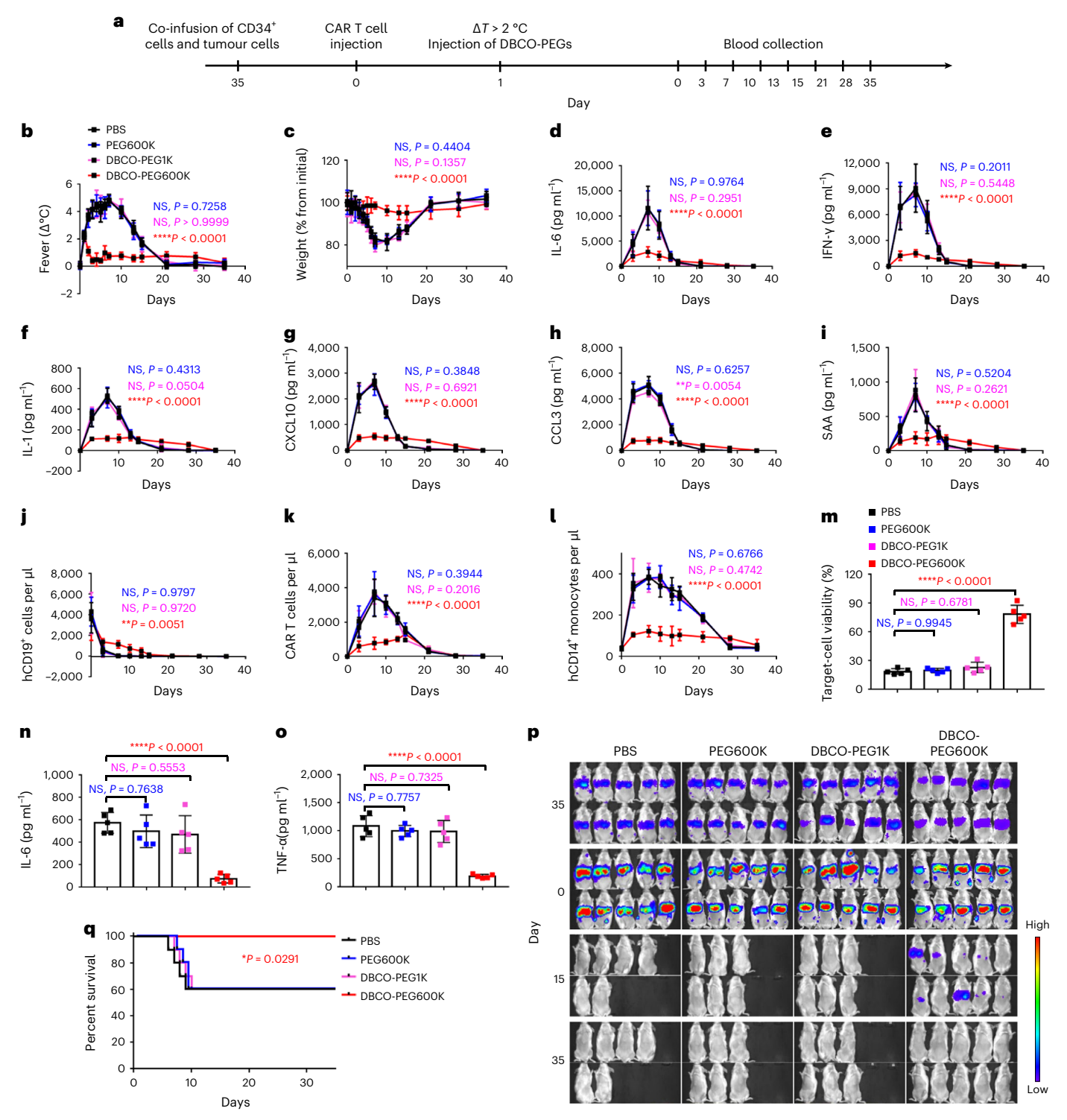


Fig. 3 | In situ PEGylation of CAR T cells alleviates cytokine release syndrome. a, CRS mouse model was constructed and mice were treated with PBS, PEG600K, DBCO-PEG1K or DBCO-PEG600K. b, c, Mouse temperature (b) and body weight (c) were monitored. d–l, The levels of IL-6 (d), IFN- γ (e), IL-1 (f), CXCL10 (g), CCL3 (h), SAA (i) and the numbers of human CD19 $^+$ cells (j), human CAR T cells (k) and human CD14 $^+$ monocytes (l) were monitored. m, CAR T cells isolated from mice were cocultured with Raji–Luc-GFP cells and monocytes, and after 24 h, Raji–Luc-GFP cell viability was determined. n, o, The levels of IL-6 (n) and TNF- α

(o) in cell-culture medium were detected. Data in \mathbf{b} - \mathbf{o} are shown as mean \pm s.d. (n = 5 biologically independent experiments, two-way ANOVA with Tukey's post hoc test). P values are indicated (blue: PEG600K versus PBS; pink: DBCO-PEG1K versus PBS; red: DBCO-PEG600K versus PBS). \mathbf{p} , In a separate animal survival experiment, the tumour-cell burden level was monitored using IVIS imaging. \mathbf{q} , Mouse survival data are shown. Exact P value indicated in the figure is from a Mantel-Cox two-sided log-rank test (n = 10 biologically independent animals). DBCO-PEG600K versus PBS, *P = 0.0291.

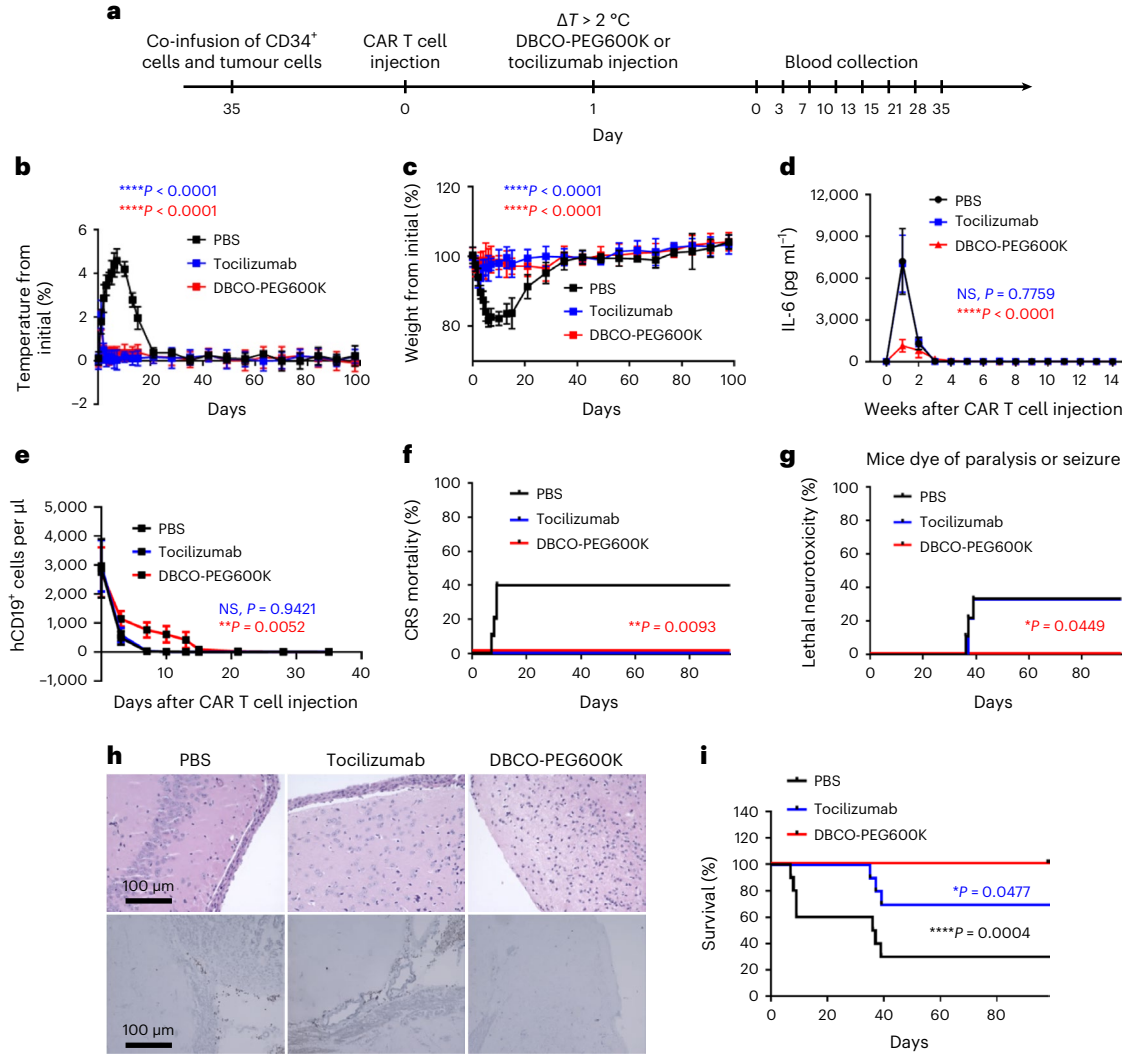


Fig. 4 | **In situ PEGylation of CAR T cells abolishes neurotoxicity. a**, Experimental timeline of construction of the CRS model and the following treatments: \mathbf{a} , 2×10^6 CAR T cells were infused into tumour-bearing mice at day 0. After the onset of high fever (day 1), mice were infused with DBCO-PEG600K (10 mg kg⁻¹) or treated with a tocilizumab in vivo bio-similar antibody (10 mg kg⁻¹). Control mice were treated with PBS. $\mathbf{b} - \mathbf{e}$, Mouse temperature (\mathbf{b}), weight (\mathbf{c}), IL-6 (\mathbf{d}) and human CD19⁺ cell levels (\mathbf{e}) in mouse blood were monitored. Data in $\mathbf{b} - \mathbf{e}$ are shown as mean \pm s.d. (n = 10 biologically independent animals, two-way ANOVA with Tukey's post hoc test). *P* values indicated in the

figure are from the comparisons on day 7 (blue: tocilizumab versus PBS; red: DBCO-PEG600K versus PBS). **f**, CRS mortality curves. **g**, Lethal neurotoxicity curves. **P** values shown in the figure are from a Mantel–Cox two-sided log-rank test. **h**, Brain haematoxylin and eosin (H&E) staining and CD68 (human) immunohistochemistry (IHC) images of mice that received different treatments at day 37. Images are representative of three independent experiments. **i**, Kaplan–Meyer survival plots. **P** values are calculated from a Mantel–Cox two-sided log-rank test: for DBCO-PEG600K versus PBS, ****P = 0.0004; for DBCO-PEG600K versus tocilizumab, *P = 0.0449.

over a tocilizumab injection to treat CRS symptoms and neurotoxicity (Fig. 4a). We found that both tocilizumab- and DBCO-PEG600K treatment can greatly control CRS-related symptoms such as high fever and weight loss (Fig. 4b–d). However, while tumour cells were completely cleared in mice that received either tocilizumab or DBCO-PEG600K by day 35 (Fig. 4e), only DBCO-PEG600K treatment substantially decreased CAR T cell expansion levels and cytokine (interferon gamma (IFN- γ), IL-6 and IL-1) production (Supplementary Fig. 17a–c). Since IL-1 is a cytokine that mainly contributes to neurotoxicity, these results demonstrate that DBCO-PEG600K could be used for neurotoxicity management.

After approximately 35 days postinjection of CAR T cells, tumour-bearing mice that received either PBS or tocilizumab developed sudden paralysis (Supplementary Fig. 17d) or seizure (Supplementary Fig. 17e), which are signs of lethal neurological syndrome²⁵. However, mice injected with DBCO-PEG600K did not show any signs of

paralysis or seizure. No signs of xenogeneic graft-versus-host disease (X-GVHD) in the skin and liver were detected according to postmortem analysis (Supplementary Fig. 18). Both to cilizumab and DBCO-PEG600K protected mice from CRS mortality (Fig. 4f) without inducing severe toxicity (Supplementary Fig. 19), but only DBCO-PEG600K prevented mice from developing lethal neurotoxicity (Fig. 4g). PBS-treated and to cilizumab-treated mice did show brain meningeal thickening (Fig. 4h) and human monocyte infiltration in the subarachnoid space (Fig. 4h). However, these were not detected in mice treated with DBCO-PEG600K. These data demonstrate that DBCO-PEG600K protected mice from severe neurotoxicity that to cilizumab was not able to protect against. As a result, only DBCO-PEG600K—and not to cilizumab—significantly prolonged mice survival (Fig. 4i).

We also asked if conjugation of PEG600K to CART cells ex vivo and infusion of the cells back into mice could treat CRS and neurotoxicity (Extended Data Fig. 1a). We constructed the Raji tumour model and

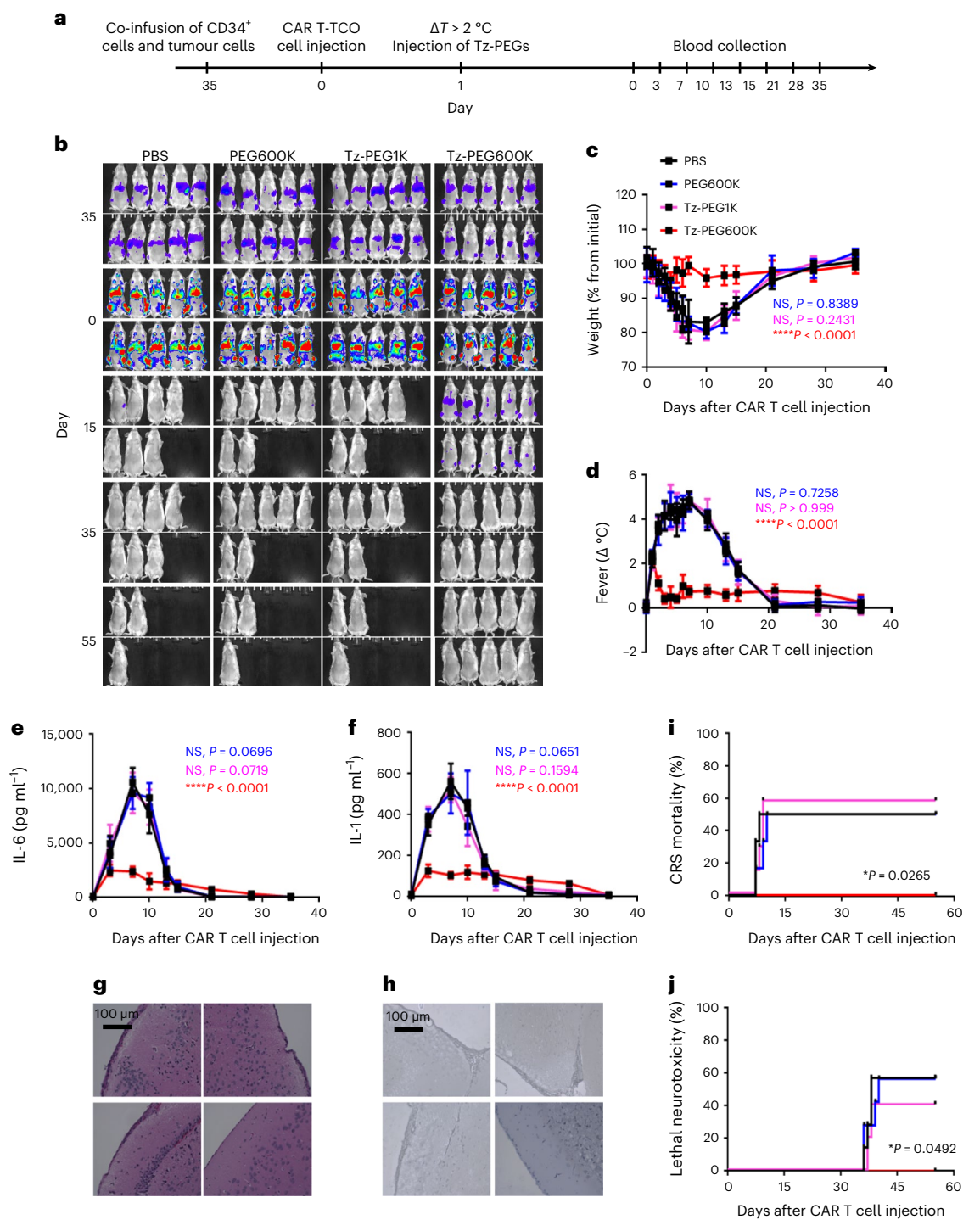


Fig. 5 | **In situ PEGylation-induced CRS and neurotoxicity alleviation can also be achieved using the tetrazine (Tz)-TCO reaction. a**, Raji tumour mouse model was constructed and TCO-modified CAR T (CAR T-TCO) cells were i.v. infused into mice on day 0. After the onset of high fever ($\Delta T > 2$ °C, day 1), PEG600K, Tz-PEG1K, Tz-PEG600K or PBS were i.v. infused into mice. **b-f**, Tumour burden (**b**), mouse body weight (**c**), temperature (**d**) and blood IL-6 (**e**) as well as IL-1 (**f**) were monitored. **g**, Brain H&E staining and **h**, human CD68 IHC images of mice that received different treatments (tissues were collected on day 37).

Images are representative of three independent experiments. **i**, CRS mortality curves. **j**, lethal neurotoxicity curves. Data in \mathbf{c} -f are shown as mean \pm s.d. (n = 10 biologically independent animals, two-way ANOVA with Tukey's post hoc test). P values indicated in the figure are from comparisons at day 7 (blue: PEG600K versus PBS; pink: Tz-PEGIK versus PBS; red: Tz-PEG600K versus PBS). Comparison in **i** and **j** was conducted using a Mantel–Cox two-sided log-rank test (n = 10). P values are indicated.

treated mice with either ex vivo PEGylated CAR T cells or regular CAR T-azide cells at day 0. On day 1, we found that mice treated with CAR T-azide cells developed high fever, so we injected DBCO-PEG600K into mice (Extended Data Fig. 1b). However, mice that received ex vivo PEGylated CAR T cells failed to develop high fever. Tumour growth was

monitored using IVIS (Extended Data Fig. 1c) and blood IL-6 (Extended Data Fig. 1d), and CART cell levels in blood (Extended Data Fig. 1e) were documented. We found that ex vivo PEGylated CART cells failed to induce IL-6 storm in mice. However, ex vivo PEGylated CART cells did not inhibit tumour growth compared with PBS treatment (Extended

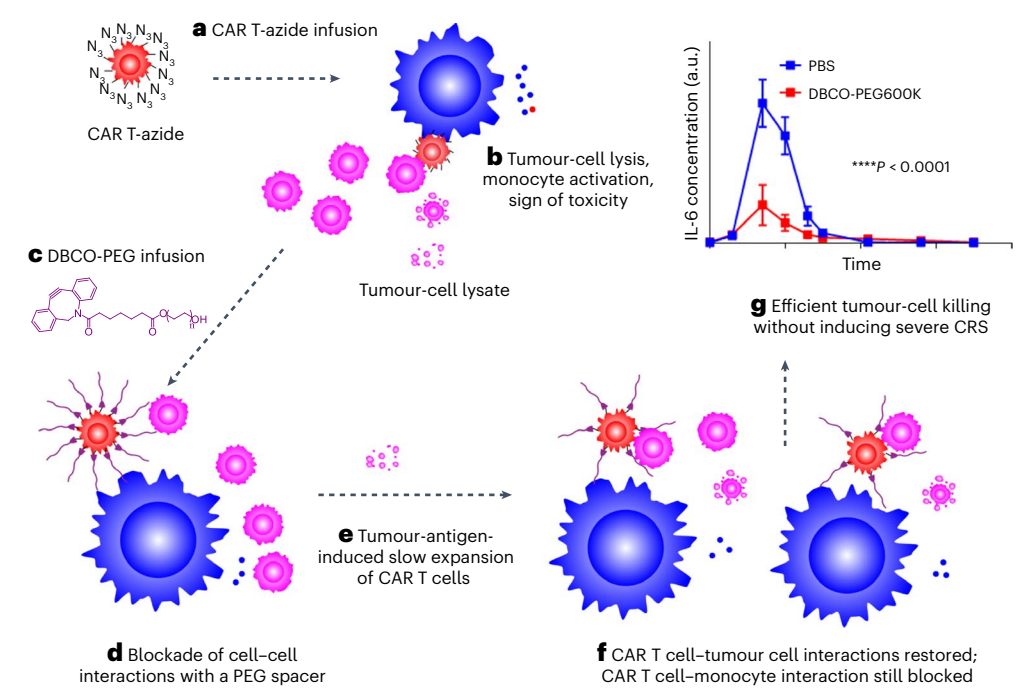


Fig. 6 | Mechanistic illustration of the in situ PEGylation strategy for managing cytokine release syndrome and neurotoxicity. a, CAR T-azide cells were infused into mice. Similar to conventional CAR T cells, they can recognize tumour cells, induce tumour-cell lysis and activate monocytes through direct cell-to-cell interactions. \mathbf{b} - \mathbf{d} , Here, upon the first signs of CRS (high fever, \mathbf{b}), DBCO-PEG600K is infused into mice, which can conjugate to the CAR T cell surface (\mathbf{c}), forming a polymeric spacer on CAR T cell surfaces to block cell-to-cell interactions (\mathbf{d}). This prevents CAR T cells and monocytes from expanding too quickly and becoming overactivated. \mathbf{e} , Over time, small tumour antigens can

reach CAR T cells to slowly activate and expand them. The PEG600K spacer on the CAR T cell surface then becomes diluted and cell-to-cell interactions are gradually restored. ${\bf f}$, CAR T cell–tumour-cell interactions are restored earlier than CAR T cell–monocyte interactions because of the relatively smaller size of B cell lymphoma cells compared with monocytes. ${\bf g}$, This creates a therapeutic window for tumour-cell killing without inducing monocyte overactivation. Data in ${\bf g}$ are shown as mean \pm s.d. (n = 10 biologically independent animals, two-way ANOVA with Tukey's post hoc test).

Data Fig. 1f). In contrast, DBCO-PEG600K treatment greatly decreased the peak IL-6 concentration and completely cleared tumour cells in vivo (Extended Data Fig. 1c). Even though the ex vivo approach did not induce CRS, the fast growth of tumour cells led to rapid mouse death (Extended Data Fig. 1g). This is because the surfaces of ex vivo PEGylated CAR T cells were fully coated with PEG, preventing the cells from reaching any tumour cells, thus prohibiting CAR T cell expansion (Extended Data Fig. 1d). However, with the in situ PEGylation strategy, the initial CAR T cell-induced cancer-cell killing led to the release of tumour antigens, which can penetrate between the PEG spacers, while slow expansion of CAR T cells restored the CAR T-tumour-cell interactions (Supplementary Fig. 16). These results demonstrate that the in situ PEGylation strategy can alleviate CAR T cell-induced CRS and neurotoxicity while not hampering tumour-killing ability.

Tetrazine-trans-cyclooctene reaction for in situ PEGylation

To explore whether this in situ PEGylation strategy could be generalized to chemistries beyond DBCO-azide, we investigated the use of the tetrazine (Tz)-trans-cyclooctene (TCO) reaction for its ability to control CAR T cell-mediated CRS and neurotoxicity (Fig. 5a–j). PEG600K, Tz-PEG1K, Tz-PEG600K, or PBS was i.v. infused into the mice. Similar to what was seen in the DBCO-azide click-chemistry-mediated in situ PEG modification (Fig. 3), treatment with Tz-PEG1K and unmodified PEG600K did not affect tumour growth, weight loss, high fever and cytokine release compared with PBS infusion (Fig. 5b–f). However, Tz-PEG600K treatment greatly reversed weight loss, high fever and cytokine release (Fig. 5c–f). Moreover, tumour cells in the Tz-PEG600K-treated mice were cleared at around day 35 post-CAR T cell injection (Fig. 5b) Further extending the duration of the experiment, we found that a

high proportion of mice in PBS-, PEG600K- and Tz-PEG1K-treated groups showed signs of neurological toxicity. However, mice in the Tz-PEG600K treated group did not show such neurological toxicity (Fig. 5g,h). Moreover, Tz-PEG600K greatly decreased CRS mortality and lethal neurotoxicity (Fig. 5i,j). Based on these results using DBCO-based click chemistry and Tz-TCO chemistry, in situ PEGylation of CART cells can act to alleviate CRS and neurotoxicity in vivo.

CART cell therapy is a revolutionary cancer immunotherapy used in the clinical setting. However, CRS and neurotoxicity restrict its broader application. In this study, we show that in situ PEGylation of CART cells (Fig. 6a-c) can greatly decrease interactions between CAR T cells, tumour cells and monocytes, which overall decreased intensive tumour-cell lysis and monocyte overactivation by CART cells (Fig. 6d). Over time, CART cells slowly expand and the PEG600K spacer becomes diluted, gradually restoring cell-to-cell interactions (Fig. 6e,f). CAR T cell-tumour-cell interactions were restored earlier than CART cellmonocyte interactions. In this way, CART cells completely clear tumour cells but do not induce severe IL-6 production (Fig. 6g). In the modern drug discovery field, researchers focus mostly on developing therapeutics for gene-, protein-, metabolic- or epigenetic-level-modulating cell behaviours. This work provides an example that disease treatment can be achieved by modulating cell-to-cell interactions with materials alone. A benefit of this system is that the polymeric spacer can be added on an as-needed basis after CART-azide cells have been administered—so that the tumour-killing ability is not dampened unless the patient presents symptoms of severe CRS. Our results demonstrate that in situ PEGylation of CART cells holds great promise for safer CAR T cell therapy. As the use of PEG may induce the generation of anti-PEG antibodies in vivo, future work will evaluate in situ conjugation of different polymers⁴⁷ or nano-/microparticles⁴⁸ as alternative 'spacers' to

control CRS and neurotoxicity. Moreover, as cell-to-cell interactions are involved in many important physiological and pathological processes⁴⁹, future studies will explore the use of in situ biomaterial-conjugation strategies to treat various diseases.

Online content

Any methods, additional references, Nature Portfolio reporting summaries, source data, extended data, supplementary information, acknowledgements, peer review information; details of author contributions and competing interests; and statements of data and code availability are available at https://doi.org/10.1038/s41563-023-01646-6.

References

- June, C. H., O'Connor, R. S., Kawalekar, O. U., Ghassemi, S. & Milone, M. C. CAR T cell immunotherapy for human cancer. Science 359, 1361–1365 (2018).
- MacKay, M. et al. The therapeutic landscape for cells engineered with chimeric antigen receptors. *Nat. Biotechnol.* 38, 233–244 (2020).
- Larson, R. C. & Maus, M. V. Recent advances and discoveries in the mechanisms and functions of CAR T cells. *Nat. Rev. Cancer* 21, 145–161 (2021).
- Mikkilineni, L. & Kochenderfer, J. N. CAR T cell therapies for patients with multiple myeloma. *Nat. Rev. Clin. Oncol.* 18, 71–84 (2021).
- Maude, S. L. et al. Chimeric antigen receptor T cells for sustained remissions in leukemia. N. Engl. J. Med. 371, 1507–1517 (2014).
- June, C. H. & Sadelain, M. Chimeric antigen receptor therapy. N. Engl. J. Med. 379, 64–73 (2018).
- Brudno, J. N. et al. T cells genetically modified to express an anti-B-cell maturation antigen chimeric antigen receptor cause remissions of poor-prognosis relapsed multiple myeloma.
 J. Clin. Oncol. 36, 2267 (2018).
- Lee, D. W. et al. Current concepts in the diagnosis and management of cytokine release syndrome. *Blood* 124, 188–195 (2014).
- Shimabukuro-Vornhagen, A. et al. Cytokine release syndrome.
 J. Immunother. Cancer 6, 1–14 (2018).
- Sterner, R. C. & Sterner, R. M. CAR-T cell therapy: current limitations and potential strategies. *Blood Cancer J.* 11, 1–11 (2021).
- Santomasso, B. D. et al. Clinical and biological correlates of neurotoxicity associated with CAR T-cell therapy in patients with B-cell acute lymphoblastic leukemia. Cancer Discov. 8, 958–971 (2018).
- 12. Cao, J.-X. et al. The incidence of cytokine release syndrome and neurotoxicity of CD19 chimeric antigen receptor–T cell therapy in the patient with acute lymphoblastic leukemia and lymphoma. Cytotherapy 22, 214–226 (2020).
- Gauthier, J. & Turtle, C. J. Insights into cytokine release syndrome and neurotoxicity after CD19-specific CAR-T cell therapy. Curr. Res. Transl. Med. 66, 50–52 (2018).
- Bonifant, C. L., Jackson, H. J., Brentjens, R. J. & Curran, K. J. Toxicity and management in CAR T-cell therapy. *Mol. Ther.-Oncolytics* 3, 16011 (2016).
- Neelapu, S. S. et al. Axicabtagene ciloleucel CAR T-cell therapy in refractory large B-cell lymphoma. N. Engl. J. Med. 377, 2531–2544 (2017).
- Davila, M. L. et al. Efficacy and toxicity management of 19-28z CAR T cell therapy in B cell acute lymphoblastic leukemia. Sci. Transl. Med. 6, 224ra225 (2014).
- Morris, E. C., Neelapu, S. S., Giavridis, T. & Sadelain, M. Cytokine release syndrome and associated neurotoxicity in cancer immunotherapy. Nat. Rev. Immunol. 22, 85–96 (2021).
- Majzner, R. G. & Mackall, C. L. Clinical lessons learned from the first leg of the CAR T cell journey. Nat. Med. 25, 1341–1355 (2019).

- Park, J. H. et al. Long-term follow-up of CD19 CAR therapy in acute lymphoblastic leukemia. N. Engl. J. Med. 378, 449–459 (2018).
- Maude, S. L. et al. Tisagenlecleucel in children and young adults with B-cell lymphoblastic leukemia. N. Engl. J. Med. 378, 439–448 (2018).
- Le, R. Q. et al. FDA approval summary: tocilizumab for treatment of chimeric antigen receptor T cell-induced severe or lifethreatening cytokine release syndrome. *Oncologist* 23, 943–947 (2018).
- Brudno, J. N. & Kochenderfer, J. N. Toxicities of chimeric antigen receptor T cells: recognition and management. *Blood* 127, 3321–3330 (2016).
- 23. Turtle, C. J. et al. CD19 CAR-T cells of defined CD4+: CD8+ composition in adult B cell ALL patients. *J. Clin. Invest.* **126**, 2123–2138 (2016).
- Giavridis, T. et al. CAR T cell-induced cytokine release syndrome is mediated by macrophages and abated by IL-1 blockade. Nat. Med. 24, 731–738 (2018).
- 25. Norelli, M. et al. Monocyte-derived IL-1 and IL-6 are differentially required for cytokine-release syndrome and neurotoxicity due to CAR T cells. *Nat. Med.* **24**, 739–748 (2018).
- Sachdeva, M., Duchateau, P., Depil, S., Poirot, L. & Valton, J. Granulocyte-macrophage colony-stimulating factor inactivation in CAR T-cells prevents monocyte-dependent release of key cytokine release syndrome mediators. *J. Biol. Chem.* 294, 5430–5437 (2019).
- 27. Frigault, M. J. et al. A phase II trial of anakinra for the prevention of CAR-T cell mediated neurotoxicity. *Blood* **138**, 2814 (2021).
- 28. Wei, J. et al. The model of cytokine release syndrome in CAR T-cell treatment for B-cell non-Hodgkin lymphoma. *Signal. Transduct. Target. Ther.* **5**, 1–9 (2020).
- Wagner, D. H. Jr, Stout, R. D. & Suttles, J. Role of the CD40-CD40 ligand interaction in CD4+ T cell contact-dependent activation of monocyte interleukin-1 synthesis. *Eur. J. Immunol.* 24, 3148–3154 (1994).
- Nashleanas, M. & Scott, P. Activated T cells induce macrophages to produce NO and control Leishmania major in the absence of tumor necrosis factor receptor p55. *Infect. Immun.* 68, 1428–1434 (2000).
- McInnes, I. B., Leung, B. P., Sturrock, R. D., Field, M. & Liew, F. Y. Interleukin-15 mediates T cell-dependent regulation of tumor necrosis factor-a production in rheumatoid arthritis. *Nat. Med.* 3, 189–195 (1997).
- Avice, M.-N., Sarfati, M., Triebel, F., Delespesse, G. & Demeure, C. E. Lymphocyte activation gene-3, a MHC class II ligand expressed on activated T cells, stimulates TNF-a and IL-12 production by monocytes and dendritic cells. *J. Immunol.* 162, 2748–2753 (1999).
- 33. Birkland, T. P., Sypek, J. P. & Wyler, D. J. Soluble TNF and membrane TNF expressed on CD4+ T lymphocytes differ in their ability to activate macrophage antileishmanial defense. *J. Leukoc. Biol.* **51**, 296–299 (1992).
- 34. Parry, S. L., Sebbag, M., Feldmann, M. & Brennan, F. M. Contact with T cells modulates monocyte IL-10 production: role of T cell membrane TNF-alpha. *J. Immunol.* **158**, 3673–3681 (1997).
- Bird, L. Calming the cytokine storm. *Nat. Rev. Immunol.* 18, 417–417 (2018).
- 36. Rooney, C. & Sauer, T. Modeling cytokine release syndrome. *Nat. Med.* **24**, 705–706 (2018).
- 37. Kolate, A. et al. PEG—a versatile conjugating ligand for drugs and drug delivery systems. *J. Control. Release* **192**, 67–81 (2014).
- Kochenderfer, J. N. et al. Eradication of B-lineage cells and regression of lymphoma in a patient treated with autologous T cells genetically engineered to recognize CD19. Blood 116, 4099–4102 (2010).

- Spiciarich, D. R. et al. Bioorthogonal labeling of human prostate cancer tissue slice cultures for glycoproteomics. *Angew. Chem. Int. Ed.* 56, 8992–8997 (2017).
- Prescher, J. A., Dube, D. H. & Bertozzi, C. R. Chemical remodelling of cell surfaces in living animals. *Nature* 430, 873–877 (2004).
- 41. Guo, C. et al. Bio-orthogonal conjugation and enzymatically triggered release of proteins within multi-layered hydrogels. *Acta Biomater.* **56**, 80–90 (2017).
- Nagahama, K., Kimura, Y. & Takemoto, A. Living functional hydrogels generated by bioorthogonal cross-linking reactions of azide-modified cells with alkyne-modified polymers. *Nat. Commun.* 9, 1–11 (2018).
- Wang, H. et al. Metabolic labeling and targeted modulation of dendritic cells. Nat. Mater. 19, 1244–1252 (2020).
- 44. Mehvar, R. Modulation of the pharmacokinetics and pharmacodynamics of proteins by polyethylene glycol conjugation. *J. Pharm. Pharm. Sci.* **3**, 125–136 (2000).
- Patel, K. et al. Use of the IL-6R antagonist tocilizumab in hospitalized COVID-19 patients. J. Intern. Med. 289, 430–433 (2020).
- 46. Hay, K. A. Cytokine release syndrome and neurotoxicity after CD 19 chimeric antigen receptor-modified (CAR-) T cell therapy. *Br. J. Haematol.* **183**, 364–374 (2018).

- 47. Nair, L. S. & Laurencin, C. T. Biodegradable polymers as biomaterials. *Prog. Polym. Sci.* **32**. 762–798 (2007).
- Acharya, G. et al. The hydrogel template method for fabrication of homogeneous nano/microparticles. J. Control. Release 141, 314-319 (2010).
- 49. Mitchell, G. & Miller, J. Cell to cell interaction in the immune response: II. The source of hemolysin-forming cells in irradiated mice given bone marrow and thymus or thoracic duct lymphocytes. *J. Exp. Med.* **128**, 821–837 (1968).

Publisher's note Springer Nature remains neutral with regard to jurisdictional claims in published maps and institutional affiliations.

Springer Nature or its licensor (e.g. a society or other partner) holds exclusive rights to this article under a publishing agreement with the author(s) or other rightsholder(s); author self-archiving of the accepted manuscript version of this article is solely governed by the terms of such publishing agreement and applicable law.

© The Author(s), under exclusive licence to Springer Nature Limited 2023

Methods

Chemicals

Polyethylene glycol (PEG) with molecular weight of 1K, 5K, 10K, 100K and 600K were purchased from Sigma, DBCO-acid was purchased from Sigma, N-azidoacetylmannosamine-tetraacylated (catalogue no. 88904) was obtained from Fisher. CD19 CAR plasmid was a gift from Scott McComb (Addgene no. 135991). The packaging plasmids pMD2.G (Addgene no. 12259) and psPAX2 (Addgene no. 12260) were from Didier Trono. CSFE dye and e450 dye were purchased from Fisher. FirePlex-96 Key Cytokines (Human) Immunoassay Panel (catalogue no. ab243549) was purchased from Abcam. Enzyme-linked immunosorbent assay kit for mouse serum amyloid A (catalogue no. KMA0021) was obtained from Thermo Fisher. Human CD68 antibody (catalogue no. 76437 S) was purchased from Cell Signalling Technology and was used as 1:1.000 dilutions. Anti-CD3 antibody (catalogue no. 85061) for T cell binding experiment was obtained from CST. Anti-human CD3-PE (catalogue no. 980008), anti-human CD4-BV711 (catalogue no. 317439), anti-human CD8-APC (catalogue no. 344721), anti-human CD19-BV711 (catalogue no. 302245) and anti-human CD14-APC (catalogue no. 325607) antibodies were purchased from Biolegend. Anti-human F(ab')₂-biotin antibody (catalogue no. 109-066-006) was purchased from Jackson ImmunoResearch. All flow antibodies were used at 1:100 dilutions. Anti-PEG antibody (ab53449) was purchased from Abcam and was used at 1:100 dilutions. StemCell EasySep human T cell isolation kit (catalogue no. 17951), Dynabead Human T-Activator CD3/CD28 (catalogue no. 11132D), retronectin (TAKARA Bio, catalogue no. T100B) and Lipofectamine 2000 (catalogue no. 11668019) were obtained from Thermo Fisher.

Cell lines and animals

Raji cells were originally ordered from ATCC (CCL-86). Raji–Luc-GFP cells were originally purchased from Creative Bio Labs (CAR-STC-ZP43). 293T cells were purchased from ATCC (CRL-3216). The cells were tested mycoplasma negative before use. Human fetal liver CD34 $^{+}$ cells were purchased from the Tissue Bank of University of Pennsylvania. Around 200 female triple transgenic NSG (SGM3) mice (6–8 weeks) expressing human stem-cell factor, granulocyte-macrophage colony-stimulating factor (GM-CSF) and IL-3 (NOD.Cg-Prkdcscid Il2rgt-m1Wjl Tg(CMV-IL3,CSF2,KITLG)1Eav/MloySzJ) were obtained from the Jackson lab and housed in a specific pathogen-free-grade animal facility with air humidity 40–70%, ambient temperature (22 \pm 2 °C) and 12-h dark/12-h light cycle. All protocols performed on animals in this study were approved by the institutional animal care and use committee of the University of Pennsylvania (protocol no. 806540).

Lentivirus production

293T cells were cultured in a 10 cm dish, and after 80% confluence was reached, the cells were treated with Opti-MEM medium containing 80 μ l lipofectamine 2000 mixed with CAR plasmid (10 μ g) and two packaging plasmids (pCMV-VSV-G, 7.5 μ g; psPAX2, 5 μ g). After 6 h, old medium was removed and 8 ml of prewarmed medium was added gently without disturbing the cells. After 24 h, virus-containing supernatant was collected and was passed through a 0.45 μ m filter. Virus-containing supernatant was then aliquoted and stored at –80 °C for further use.

Preparation of CART cells

Some 24-well untreated plates were treated with 20 μ g ml⁻¹ of Retronectin in PBS at 4 °C overnight. Then lentiviral supernatants were added, and the plate was centrifuged at 1,000g for 1 h for lentiviral adhesion. The spleens of humanized mice were collected, and CD8+T cells were isolated using a human CD8+T cell isolation kit. T cells were activated with Dynabeads Human T-Activator CD3/CD28 at a bead-to-cell ratio of 1:1, and 50 IU ml⁻¹ recombinant IL-2 was added to the cell-culture medium. After 48 h of activation, Dynabeads were removed, and the T cells were added to lentiviral-coated 24-well plates (1 million cells

per well). At 2 days after T cells were added, transduction efficiencies were determined by flow.

Synthesis of DBCO-PEG

Dibenzocyclooctyne (DBCO)-acid was mixed with PEG 1K, 5K, 10K, 100K or 600K in dichloromethane (DCM) under $\rm N_2$ protection, N-ethyl-N'-(3-dimethylaminopropyl)carbodiimide hydrochloride (EDC) and 4-(dimethylamino)pyridine (DMAP) were used as catalysts. After 24 h, DCM was removed under reduced pressure and the free DBCO-acid and catalysts were removed by dialysis.

Azido glycans modification on CART cell surfaces

The surfaces of CART cells were labelled with azido glycans by culturing CART cells with Ac4ManNAz for 48 h. Confocal images were obtained using a Ziess LSM 710 confocal with ZEN2010 software.

$Construction\ of\ humanized\ immune\ system\ NSG-SGM3\ mouse\ model$

Recently, a study developed a murine model of CRS, where they found that CART cells injected into humanized mice bearing leukaemia can induce severe CRS and neurotoxicity²⁵. Here, we also constructed a humanized mouse model following their method, with modification. NSG-SGM3 mice were treated with busulfan (40 mg kg⁻¹) to remove the bone marrow, and then 10⁵ human fetal liver CD34⁺ cells were i.v. injected into mice. The development of human immune cells including T cells, B cells and monocytes in blood was determined by flow cytometry and histological analysis. X-GVHD was monitored for daily by assessing mouse activity, weight loss, fur texture and skin integrity. To construct the CRS model in tumour-bearing mice, 1 × 10⁴ Raji cells and 1 × 10⁵ human fetal liver CD34⁺ cells were co-infused into NSG-SGM3 mice to develop human immune cells and to allow tumour growth. After 7 weeks, 2 × 106 human T cells isolated from a non-tumour-bearing humanized mouse were transduced with CD19 CAR (1928z). These cells were then injected i.v. into tumour-bearing mice. Body weight and temperature were recorded every 3 days. Blood was also collected to determine the levels of various cytokines and the numbers of tumour cells, CAR T cells and monocytes. The concentrations of several human cytokines, such as interleukin 6 (IL-6), IL-1, tumour necrosis factor alpha (TNF-α), IL-8 and mouse serum amyloid A (SAA, a murine homologue to the human CRS biomarker C-reactive protein) in the blood were also monitored. Mouse IL-6 and TNF-α levels were also measured. CRS mortality was defined as death preceded by the following criteria: more than 20% body weight loss, $\Delta T > 2$ °C and serum IL-6 > 2,500 pg ml⁻¹. Neurotoxicity-induced lethality was defined as death in the absence of CRS criteria and preceded by either seizures or paralysis. The maximal tumour size/burden permitted by the ethics committee is 2 cm; we confirmed that during this study the size limit was not reached.

Flow cytometry and cell sorting experiments

A total of 50–100 μl mouse blood was collected in ethylenediamineter-raacetic acid (EDTA)-pretreated tubes using the orbital bleeding method. Cells were spun down, the red blood cells were lysed with ACK lysing buffer, and the cell suspensions were passed through a 70 μm cell strainer before being stained with antibodies for flow cytometry (BD LSR II). CAR T cell sorting from mouse blood was performed using a BD FACSAria.

IVIS imaging

Raji–Luc-GFP tumour growth in mice was monitored using a Perkin Elmer in vivo imaging system (IVIS, Lumina 3). Mice were intraperitoneally injected with *D*-luciferin (150 mg kg⁻¹) for 15 min, and then were imaged in the IVIS system under inhaled isoflurane anaesthesia.

Statistics

Statistical analysis was performed using Graphpad prism v.7.0 software. Error bars represent mean ± standard deviation (s.d.). One- or two-way analyses of variance (ANOVAs) were used as appropriate to compare

means, with Tukey's post hoc test. The differences in animal survival experiments were calculated using the Kaplan–Meyer method and the P values were determined using the log-rank test.

Reporting summary

Further information on research design is available in the Nature Portfolio Reporting Summary linked to this article.

Data availability

All relevant data of this study are available within the paper and its Supplementary Information files. Source data are provided with this paper.

Acknowledgements

M.J.M. acknowledges support from an NIH Director's New Innovator Award (no. DP2TR002776), an NSF CAREER Award (no. CBET-2145491), a Burroughs Wellcome Fund Career Award at the Scientific Interface and the American Cancer Society (no. RSG-22-122-01-ET). The authors thank the June lab for the help on CAR T cell preparation. The authors also acknowledge the NIH S10 grant (1S100D026986) for the support on a cell sorter.

Author contributions

N.G. and M.J.M. conceived and designed the experiments. N.G., X.H., L.X. and A.G.H. performed the experiments. N.G., L.X., X.H. and R.E.M.

analysed the data. N.G. and M.J.M. wrote the manuscript. M.M.B. and A.E.M. edited the manuscript. All authors discussed the results and commented on the manuscript.

Competing interests

N.G. and M.J.M. have filed a patent application related to this study. The remaining authors declare no competing interests.

Additional information

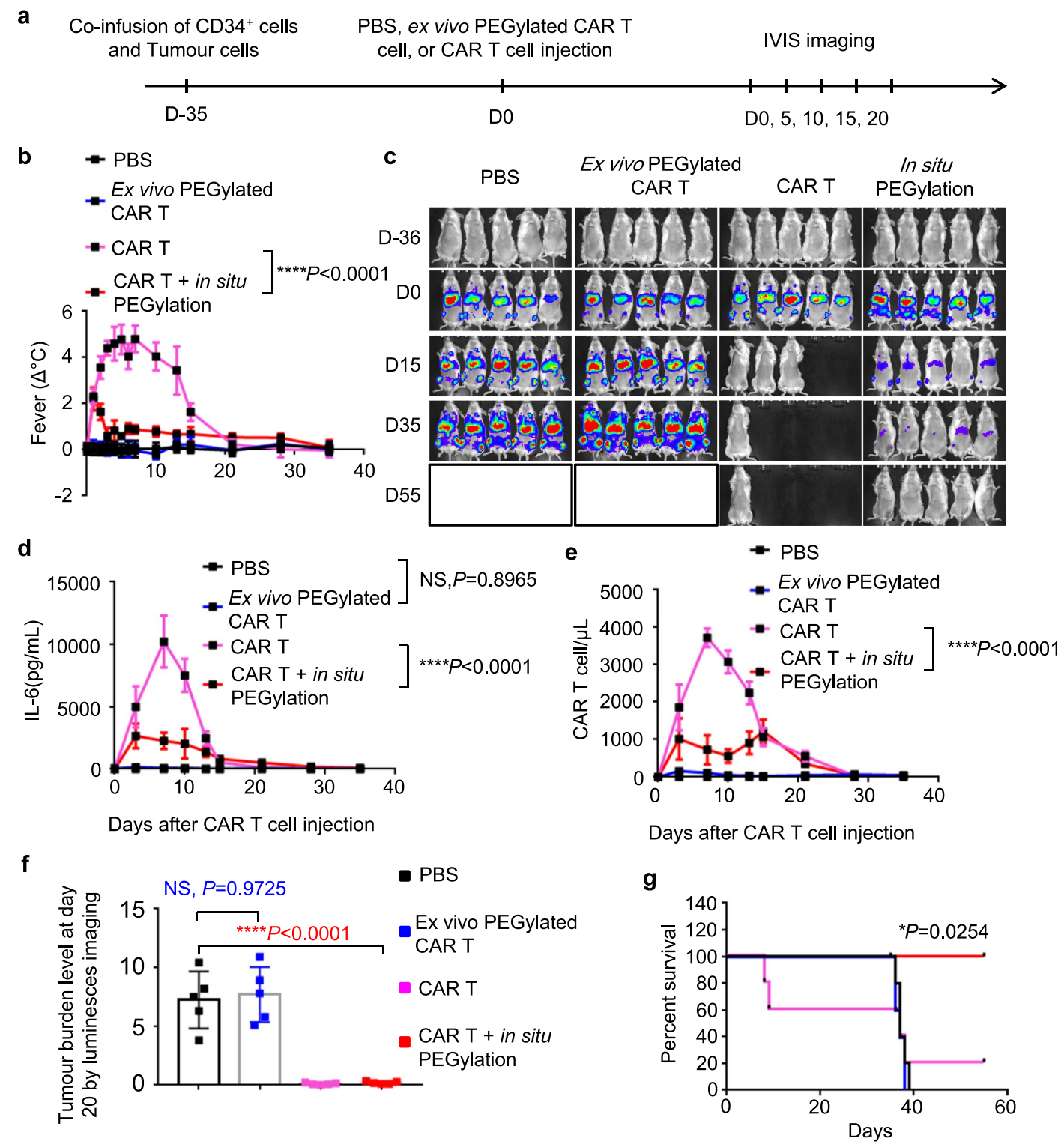
Extended data is available for this paper at https://doi.org/10.1038/s41563-023-01646-6.

Supplementary information The online version contains supplementary material available at https://doi.org/10.1038/s41563-023-01646-6.

Correspondence and requests for materials should be addressed to Michael J. Mitchell.

Peer review information *Nature Materials* thanks Bruno De Geest, Christopher Jewell and the other, anonymous, reviewer(s) for their contribution to the peer review of this work.

Reprints and permissions information is available at www.nature.com/reprints.



Extended Data Fig. 1| **Comparison of the CAR T cell ex vivo PEGylation strategy with the in situ PEGylation strategy. a**, Raji tumour-bearing mouse model was constructed, and mice were treated with either ex vivo PEGylated CAR T cells or regular CAR T-azide cells at day 0. On day 1, the mice receiving regular CAR T-azide cells developed high fever ($\Delta T > 2$ °C), after which DBCO-PEG600k (in situ PEGylation) was injected. Mouse body temperature (**b**), tumour burden (**c**), blood IL-6 levels (**d**) and CAR T cell levels (**e**) were monitored. **f**, quantification

of tumour burden in different groups at day 35. **g**, Kaplan–Meyer survival plots. Data in (\mathbf{b}) , (\mathbf{d}) , (\mathbf{e}) , and (\mathbf{f}) are shown as mean \pm s.d. (n=5). Statistical differences in (\mathbf{b}) , (\mathbf{d}) , and (\mathbf{e}) were calculated using two-way ANOVA with Tukey's post hoc test. Statistical differences in (\mathbf{f}) were calculated using one-way ANOVA with Tukey's post hoc test. P values indicated in the figure are from the comparisons on day 7. Statistical differences in (\mathbf{g}) were conducted using a Mantel–Cox two-sided log-rank test (n=5). P values are indicated.

nature portfolio

Corresponding author(s):	Michael Mitchell
Last updated by author(s):	Jul 1, 2023

Reporting Summary

Nature Portfolio wishes to improve the reproducibility of the work that we publish. This form provides structure for consistency and transparency in reporting. For further information on Nature Portfolio policies, see our <u>Editorial Policies</u> and the <u>Editorial Policy Checklist</u>.

For all statistical analyses, confirm that the following items are present in the figure legend, table legend, main text, or Methods section

_				•
	- ~	+-	\sim \pm	ics
_ \	_		\sim 1	и <

. 0.	an statistical analyses, commit that the following terms are present in the figure regend, table regend, main text, or internous section.
n/a	Confirmed
	\square The exact sample size (n) for each experimental group/condition, given as a discrete number and unit of measurement
	A statement on whether measurements were taken from distinct samples or whether the same sample was measured repeatedly
	The statistical test(s) used AND whether they are one- or two-sided Only common tests should be described solely by name; describe more complex techniques in the Methods section.
	A description of all covariates tested
	A description of any assumptions or corrections, such as tests of normality and adjustment for multiple comparisons
	A full description of the statistical parameters including central tendency (e.g. means) or other basic estimates (e.g. regression coefficient) AND variation (e.g. standard deviation) or associated estimates of uncertainty (e.g. confidence intervals)
	For null hypothesis testing, the test statistic (e.g. <i>F</i> , <i>t</i> , <i>r</i>) with confidence intervals, effect sizes, degrees of freedom and <i>P</i> value noted <i>Give P values as exact values whenever suitable.</i>
\boxtimes	For Bayesian analysis, information on the choice of priors and Markov chain Monte Carlo settings
\boxtimes	For hierarchical and complex designs, identification of the appropriate level for tests and full reporting of outcomes
\boxtimes	Estimates of effect sizes (e.g. Cohen's <i>d</i> , Pearson's <i>r</i>), indicating how they were calculated
	Our web collection on <u>statistics for biologists</u> contains articles on many of the points above.
So	ftware and code

Policy information about <u>availability of computer code</u>

Data collection ZEN2010, MestReNova 9.0, Flowjo V10, IVIS specturm 4.4, BD FACSAria

Data analysis Statistical analysis were performed on Graphpad Prism 7.0, flowcytometry data were analyzed on FlowJo software package (Flowjo V10).

For manuscripts utilizing custom algorithms or software that are central to the research but not yet described in published literature, software must be made available to editors and reviewers. We strongly encourage code deposition in a community repository (e.g. GitHub). See the Nature Portfolio guidelines for submitting code & software for further information.

Data

Policy information about availability of data

All manuscripts must include a data availability statement. This statement should provide the following information, where applicable:

- Accession codes, unique identifiers, or web links for publicly available datasets
- A description of any restrictions on data availability
- For clinical datasets or third party data, please ensure that the statement adheres to our policy

All relevant data of this study are available within the paper and its Supplementary Information files. A dataset is provided.

Human rese	arch narti	cinants			
		nvolving human research participants and Sex and Gender in Research.			
Reporting on sex	and gender	N/A			
Population characteristics		N/A			
Recruitment		N/A			
		N/A			
	ation on the appr	roval of the study protocol must also be provided in the manuscript.			
Field-spe	cific re	porting			
	ne below that i	s the best fit for your research. If you are not sure, read the appropriate sections before making your selection.			
Life sciences		Behavioural & social sciences Ecological, evolutionary & environmental sciences			
For a reference copy of t	he document with	all sections, see nature.com/documents/nr-reporting-summary-flat.pdf			
Life scier	nces sti	udy design			
All studies must dis	close on these	points even when the disclosure is negative.			
Sample size	No effect size was predetermined, but sample sizes employed in this study are consistent with previously published works (Li A W, Sobral M C, Badrinath S, et al. Nature materials, 2018, 17(6): 528-534; or Kuai R, Ochyl L J, Bahjat K S, et al. Nature materials, 2017, 16(4): 489-496.). For example, in vitro studies were repeated at least three times independently and in the in vivo experiments with 7-10 mice per group were performed.				
Data exclusions	No animals and	d/or data were excluded.			
Replication	All experiment	s were repeated for at least three times and experimental findings were reproducible.			
Randomization	For animal experiments, dosing groups were filled by randomly selecting from the same pool of animals. Groups in all the in vitro and in vivo experiments were selected randomly.				
Blinding	All the investigators were blinded to group allocation during data collection and analysis.				
We require information	on from authors	Decific materials, systems and methods about some types of materials, experimental systems and methods used in many studies. Here, indicate whether each material, your study. If you are not sure if a list item applies to your research, read the appropriate section before selecting a response.			
Materials & exp	perimental s	ystems Methods			
<u>' </u>		n/a Involved in the study			
Antibodies		ChIP-seq			
Eukaryotic cell lines Palaeontology and archaeology		logy MRI-based neuroimaging			
Animals and other organisms					

Antibodies

Antibodies used

Clinical data

Dual use research of concern

Anti-human CD68 antibody (Catalog# 76437S, clone# D4B9C, 1:1000 dilution) and anti-human CD3 antibody (Catalog# 85061, clone# D7A6E, 1:1000 dilution) were obtained from Cell Signaling Technology. Anti-human CD3-PE (Catalog: 980008, clone# UCHT1, 1:100 dilution), anti-human CD4-BV711 (Catalog: 317439, clone# OKT4, 1:100 dilution), anti-human CD8-APC (Catalog: 344721, clone# SK1, 1:100 dilution), anti-human CD19-BV711 (Catalog: 302245, clone# HIB19, 1:100 dilution), and anti-human CD14-APC (Catalog: 302245, clone# HIB19, 1:100 dilution), and anti-human CD14-APC (Catalog: 302245, clone# HIB19, 1:100 dilution), and anti-human CD14-APC (Catalog: 302245, clone# HIB19, 1:100 dilution), and anti-human CD14-APC (Catalog: 302245, clone# HIB19, 1:100 dilution), and anti-human CD14-APC (Catalog: 302245, clone# HIB19, 1:100 dilution), and anti-human CD14-APC (Catalog: 302245, clone# HIB19, 1:100 dilution), and anti-human CD14-APC (Catalog: 302245, clone# HIB19, 1:100 dilution), and anti-human CD14-APC (Catalog: 302245, clone# HIB19, 1:100 dilution), and anti-human CD14-APC (Catalog: 302245, clone# HIB19, 1:100 dilution), and anti-human CD14-APC (Catalog: 302245, clone# HIB19, 1:100 dilution), and anti-human CD14-APC (Catalog: 302245, clone# HIB19, 1:100 dilution), and anti-human CD14-APC (Catalog: 302245, clone# HIB19, 1:100 dilution)

325607, clone# HCD14, 1:100 dilution) antibodies were purchased from Biolegend. Anti-human F(ab¹)₂ fragment- DyLight™ 405 antibody (Catalog: 109-475-006, clone# Polyclonal, 1:100 dilution) was purchased from Jackson ImmunoResearch. Anti-PEG antibody (Catalog: ab53449, 1:100 dilution) was purchased from Abcam.

Validation

All the antibodies used are from commercial sources and have been validated by the vendors. Validation data are available on the manufacturer's website

- 1. Anti-human CD68 antibody has been validated to be used for Immunohistochemistry analysis and mentioned species reactivity with human. (ref. Fan C S, et al. Oncotarget, 2018, 9(4): 4998. DOI: 10.18632/oncotarget.23578)
- 2. Anti-human CD3 antibody has been validated to be used for Immunohistochemistry analysis and mentioned species reactivity with human (ref. Gong T J, Frontiers in Oncology, 2021, 11: 728437. DOI: 10.3389/fonc.2021.728437)
- 3. Anti-human CD3-PE antibody has been validated to be used for flow cytometric analysis and mentioned species reactivity with human. (Data is provided on their website: https://www.biolegend.com/en-us/products/pe-anti-human-cd3-antibody-17523)
- 4. Anti-human CD4-BV711 antibody has been validated to be used for flow cytometric analysis and mentioned species reactivity with human. (Data is provided on their website: https://www.biolegend.com/en-us/products/brilliant-violet-711-anti-human-cd4-antibody-7942)
- 5. Anti-human CD8-APC antibody has been validated to be used for flow cytometric analysis and mentioned species reactivity with human. (Data is provided on their website: https://www.biolegend.com/en-us/products/apc-anti-human-cd8-antibody-6531)
 6. Anti-human CD19-BV711 antibody has been validated to be used for flow cytometric analysis and mentioned species reactivity with human. (Data is provided on their website: https://www.biolegend.com/en-us/products/brilliant-violet-711-anti-human-cd19-antibody-8519)
- 7. Anti-human CD14-APC antibody has been validated to be used for flow cytometric analysis and mentioned species reactivity with human. (Data is provided on their website: https://www.biolegend.com/en-us/products/apc-anti-human-cd14-antibody-3953) 8. Anti-human F(ab')₂ fragment-Biotin antibody has been validated to be used for flow cytometric analysis and mentioned species reactivity with human. (Data is provided on their website: https://www.jacksonimmuno.com/catalog/products/109-066-006. Also in this paper: Guo X, et al. Frontiers in pharmacology, 2018, 9: 1118. DOI: 10.3389/fphar.2018.01118)
- 9. Anti-PEG antibody has been validated to be used for flow cytometric analysis. (Data is provided on their website: https://www.jacksonimmuno.com/catalog/products/109-066-006 https://www.abcam.com/products/primary-antibodies/biotin-polyethylene-glycol-antibody-peg-b-47b-ab53449.html)

Eukaryotic cell lines

Policy information about cell lines and Sex and Gender in Research

oncy information about <u>cell lines and Sex and Gender in Nesearch</u>

Raji cells were originally ordered from ATCC (CCL-86). Raji-Luc-GFP cells were originally from Creative Bio Labs (CAR-STC-ZP43). 293T cells were purchased from ATCC (CRL-3216). and all of the cell lines were tested negative for mycoplasma in University of Pennsylvania cell center.

Authentication

Cell line source(s)

Raji cells were authenticated by ATCC (https://www.atcc.org/products/ccl-86)
Raji-Luc-GFP cells were authenticated by Creative Bio Labs (https://www.creative-biolabs.com/car-t/human-burkitt-lymphoma-cell-line-raji-luciferase-gfp-puro-overexpressed-93090.htm?gclid=Cj0KCQjw4s-kBhDqARlsAN-ipH0WVOey3g_YN0rmwPP8VBZ7iqW92Bnh5L00KkUwe4g2xY_MvDZDAKkaApaaEALw_wcB)
293T cells were authenticated by ATCC (https://www.atcc.org/products/crl-3216?nt=wobj-20-q)

Mycoplasma contamination

All cell lines were tested for mycoplasma contamination. No mycoplasma contamination was found.

Commonly misidentified lines (See ICLAC register)

Raji, Raji-luc-gfp cell lines cell lines are not listed in the database.

Animals and other research organisms

Policy information about <u>studies involving animals</u>; <u>ARRIVE guidelines</u> recommended for reporting animal research, and <u>Sex and Gender in Research</u>

Laboratory animals

Around 200 Female Ttriple transgenic NSG (SGM3) mice (6-8 week) expressing human stem cell factor, granulocyte-macrophage colony-stimulating factor (GM-CSF) and IL-3 (NOD.Cg-Prkdcscid Il2rgtm1Wjl Tg(CMV-IL3,CSF2,KITLG)1Eav/MloySzJ) were obtained from the Jackson lab and were housed in a specific pathogen free-grade animal facility with air humidity 40%–70%, ambient temperature (22 \pm 2 °C), and 12-h dark/12-h light cycle.

Wild animals

No wild animal was used in this study.

Reporting on sex

Female mice were used in this study

Field-collected samples

The study did not involve samples collected from field.

Ethics oversight

All animal experiment protocols were reviewed and approved by the institutional animal care and use committee of the University of Pennsylvania.

Note that full information on the approval of the study protocol must also be provided in the manuscript.

Flow Cytometry

Plots

Confirm that:

- The axis labels state the marker and fluorochrome used (e.g. CD4-FITC).
- The axis scales are clearly visible. Include numbers along axes only for bottom left plot of group (a 'group' is an analysis of identical markers).
- All plots are contour plots with outliers or pseudocolor plots.
- A numerical value for number of cells or percentage (with statistics) is provided.

Methodology

Sample preparation

Mice blood was incubated with ammonium chloride buffer for erythocyte lysis and washed with PBS. Single-cell suspensions were obtained by filtering through a 70 µM cell strainer. Then the suspensions and stained with antibodies according to the manufacturer's protocols, and then analyzed by flow cytometry.

Instrument BD LSR II

Software PlowJo software package (Flowjo V10)

Cell population abundance The absolute cells around 8000-10000 were analyzed for fluorescent intensity in the defined gate.

Gating strategy

In general, cells were first gated on FSC/SSC. Singlet cells were gated using FSC-H and FSC-A. Dead cells were then excluded and further surface and intracellular antigen gating was performed on the live cell population (Supplementary Figure 23).

| Tick this box to confirm that a figure exemplifying the gating strategy is provided in the Supplementary Information.